

# Canes Venatici I cloud of galaxies seen in the $H\alpha$ line

S.S. Kaisin and I.D. Karachentsev

Special Astrophysical Observatory, Russian Academy of Sciences, N. Arkhyz, KChR, 369167, Russia

Preprint online version: October 31, 2018

## ABSTRACT

We present results of  $H\alpha$  imaging for 42 galaxies in the nearby low-density cloud Canes Venatici I populated mainly by late-type objects. Estimates of the  $H\alpha$  flux and integrated star formation rate ( $SFR$ ) are now available for all 78 known members of this scattered system, spanning a large range in luminosity, surface brightness,  $HI$  content and  $SFR$ . Distributions of the CVnI galaxies versus their  $SFR$ , blue absolute magnitude and total hydrogen mass are given in comparison with those for a population of the nearby virialized group around M81. We found no essential correlation between star formation activity in a galaxy and its density environment. A bulk of CVnI galaxies had enough time to generate their baryon mass with the observed  $SFR$ . Most of them possess also a supply of gas sufficient to maintain their observed  $SFR$ s during the next Hubble time.

**Key words.** galaxies:evolution — galaxies:ISM — galaxies:dwarfs

## 1. Introduction

The distribution over the sky of 500 galaxies of the Local volume with distances within 10 Mpc shows considerable inhomogeneities due to the presence of groups and voids. Apart from several virialized groups, like the group around the galaxy M81, an amorphous association of nearby galaxies in the Canes Venatici constellation was noted by many authors (Karachentsev 1966, de Vaucouleurs 1975, Vennik 1984, Tully 1988). The boundaries of it are rather uncertain. Roughly, in a circle of radius  $\sim 20^\circ$  around the galaxy NGC 4736 there are about 80 known galaxies with  $D < 10$  Mpc, which corresponds to a density contrast on the sky  $\Delta N/N \sim 4$ . Inside of this complex the distribution of galaxies is also inhomogeneous, showing some clumps differing in their location on the sky and distances in depth. About 70% of the population of the cloud accounts for irregular dwarf galaxies, whose masses are obviously insufficient to keep such a system in the state of virial equilibrium. As data on distances of galaxies accumulated, a possibility appeared of studying the kinematics of the cloud in details. As was shown by Karachentsev et al. (2003), the CVnI cloud is in a state close to the free Hubble expansion, having a characteristic crossing time of about 15 Gyr.

Being a scattered system with rare interactions between galaxies, the nearby CVnI cloud is a unique laboratory for studying star formation processes in galaxies running independently, without a noticeable external influence. Kennicutt et al. (1989), Hoopes et al. (1999), van Zee (2000), Gil de Paz et al. (2003), James et al. (2004) and Hunter & Elmegreen (2004) conducted observations in the  $H\alpha$  line of three dozen galaxies of this complex, which made it possible to determine the star formation rate ( $SFR$ ) in them. However, more than half of other members of the cloud proved to be out of vision of these authors. Our task consisted in the completion of  $H\alpha$ -survey of the population of the CVnI cloud. The results of our observations and their primary analysis are presented in this paper.

## 2. Observations and data reduction

CCD images in the  $H\alpha$ -line and continuum were obtained for 42 galaxies of the CVnI cloud during observing runs from 2001 March to 2006 May. An average seeing was  $1.8''$ . All the observations were performed in the Special Astrophysical Observatory of the Russian Academy of Sciences with the BTA 6-m telescope equipped with the SCORPIO focal reducer (Afanasiev et al. 2005). A CCD chip of  $2048 \times 2048$  pixels provides a total field of view of about  $6.1'$  with a scale of  $0.18''/\text{pixel}$ . The images in  $H\alpha + [\text{NII}]$  and continuum were obtained via observing the galaxies through a narrow-band interference filter  $H\alpha(\Delta\lambda = 75\text{\AA})$  with an effective wavelength  $\lambda = 6555\text{\AA}$  and two medium-band filters for the continuous spectrum SED607 with  $\Delta\lambda = 167\text{\AA}$ ,  $\lambda = 6063\text{\AA}$  and SED707 with  $\Delta\lambda = 207\text{\AA}$ ,  $\lambda = 7063\text{\AA}$ , respectively. Typical exposure times for the galaxies were  $2 \times 300\text{s}$  in the continuum and  $2 \times 600\text{s}$  in  $H\alpha$ . Since the range of radial velocities in our sample is small, we used one and the same  $H\alpha$  filter for all the observed objects. Table 1 presents a brief synopsis of these runs, where columns are: (1) the galaxy name, (2) the date of observation, (3) the total exposure time in seconds; a colon means that the sky was not photometric. Our data reduction followed the standard practice and was performed within the MIDAS package. For all the data bias was subtracted and the images were flat-fielded by twilight flats. Cosmic particles were removed and the sky background was subtracted. The next operation was to bring all the images of a given object into coincidence. Then the images in the continuum were normalized to  $H\alpha$  images using 5–15 field stars and subtracted.  $H\alpha$  fluxes were obtained for the continuum-subtracted images, using spectrophotometric standard stars from Oke (1990) observed in the same nights as the objects. The investigation of measurement errors contributed from the continuum subtraction, flat-fielding and scatter in the zeropoints has shown that they have typical values within 10%. We did not correct  $H\alpha$

fluxes for the contribution of the [NII] lines, because it is likely to be small for the majority of low-luminosity galaxies in our sample.

### 3. Results

The images of 42 galaxies that we obtained in the CVnI cloud are displayed in the form of mosaic in Fig.1. The left and right image of every galaxy corresponds to the sum and difference of the frames exposed in  $H\alpha$  and continuum. The frame size is about  $4' \times 4'$ , the North and East directions are indicated by the arrows, the scale is denoted in the lower right angle.

Some basic properties of 78 galaxies located in the CVnI cloud are listed in Table 2. It also includes the data on the galaxies that were observed by other authors earlier. The columns of Table 2 contain the following characteristics of the cloud members taken mainly from the Catalog of Neighboring Galaxies (CNG); Karachentsev et al. 2004: (1) the galaxy name, (2) and (3) the equatorial coordinates for the epoch J2000.0, (4) morphological type in numerical code according to de Vaucouleurs et al. (1991), (5) the tidal index ( $TI$ ) following from the CNG; i.e. for every galaxy “ $i$ ” we have found its “main disturber” (=MD), producing the highest tidal action  $TI_i = \max\{\log(M_k/D_{ik}^3)\} + C$ , ( $k = 1, 2, \dots, N$ ), where  $M_k$  is the total mass of any neighboring potential MD galaxy (proportional to its luminosity with  $M/L_B = 10M_\odot/L_\odot$ ) separated from the considered galaxy by a space distance  $D_{ik}$ ; the value of the constant  $C$  is chosen so that  $TI = 0$ , when the Keplerian cyclic period of the galaxy with respect to its MD equals the cosmic Hubble time,  $T_0$ ; therefore positive values correspond to galaxies in groups, while the negative ones correspond to field galaxies. Column (6) gives the galaxy radial velocity (in  $\text{km s}^{-1}$ ) with respect to the Local Group centroid with the apex parameters adopted in the NASA/IPAC Extragalactic Database (NED). Column (7) gives the distance to a galaxy in megaparsecs with allowance made for new measurements (Karachentsev et al. 2006, Tully et al. 2007). Column (8) presents the blue absolute magnitude of a galaxy with the given distance after correction for the Galactic extinction  $A_b$  from Schlegel et al. (1998) and the internal absorption in the galaxy determined as  $A_{int} = [1.6 + 2.8(\log V_m - 2.2)] \cdot \log(a/b)$ , if  $V_m > 42.7 \text{ km s}^{-1}$ , otherwise,  $A_{int} = 0$ . Here,  $V_m$  is the rotation velocity of the galaxy corrected for the inclination, and  $a/b$  is the galaxy axial ratio. Therefore, we assume the internal absorption to be dependent not only on the inclination, but also on the galaxy luminosity (Verheijen, 2001). Column (9) gives the logarithm of the hydrogen mass of a galaxy,  $\log(M_{HI}/M_\odot) = \log F_{HI} + 2 \lg D_{Mpc} + 5.37$ , defined from its flux  $F_{HI}$  in the 21 cm line; in some dwarf spheroidal galaxies the upper limit of the flux was estimated from the observations by Huchtmeier et al. (2000). Column (10) gives the logarithm of the observed integral flux of a galaxy in the  $H\alpha$  + [NII] lines expressed in terms of  $\text{erg cm}^{-2}\text{sec}^{-1}$ . Notes indicate data sources of  $SFR$ s according to other authors. Column (11) gives the star formation rate in the galaxy on a logarithmic scale,  $SFR(M_\odot/\text{year}) = 1.27 \cdot 10^9 F_c(H\alpha) \cdot D^2$  (Gallagher et al. 1984), where the integral flux in the  $H\alpha$  line is corrected for the Galactic and internal extinction as  $A(H\alpha) = 0.538 \cdot A_b$ , while the galaxy distance is expressed in Mpc. Columns (12) and (13) give the dimensionless parameters  $p_* = \log([SFR] \cdot T_0/L_B)$  and

$f_* = \log(M_{HI}/[SFR] \cdot T_0)$ , which characterize the past and the future of the process of star formation; here  $L_B$  denotes the total blue luminosity of galaxy in units of solar luminosity, while  $T_0$  is the age of the universe assumed equal to 13.7 billion years (Spergel et al. 2003). Here we note some properties of the galaxies that we observed, in particular, their  $HII$  pattern.

*UGC 5427.* This dwarf galaxy with asymmetric  $HII$  filaments is situated at the farthest western outskirts of the CVnI cloud. Its distance, 7.1 Mpc, was estimated from the luminosity of the brightest stars.

*NGC 3344.* This is one of the rare galaxies in the cloud with a quite regular spiral pattern. Its distance of 6.9 Mpc determined from the radial velocity at a Hubble constant  $H_0 = 72 \text{ km s}^{-1}\text{Mpc}^{-1}$  may be considerably underestimated since the galaxy is located in the Local Velocity Anomaly zone (Tully et al. 1992).

*KK 109.* This dwarf system of low surface brightness belongs to an intermediate type between irregular and spheroidal galaxies like the known member of the Local Group, LGS-3. Its distance, 4.51 Mpc, was determined from the tip of the red giant branch, TRGB (Karachentsev et al. 2003). There are no massive neighbors ( $TI = -0.6$ ) in the vast vicinities of KK 109, which could cause pushing of gas from this galaxy by the ram pressure. The  $H\alpha$ -flux shown in Table 2 for the galaxy corresponds only to the upper limit.

*BTS 76 and MGC 6-27-17.* These are two relatively compact bluish galaxies the shape of which is not notable for great irregularity. They have not been resolved into stars yet, and the distances to them are estimated from their radial velocities. In the central parts of both galaxies compact emission knots are seen.

*DDO 113 = KDG 90.* This is a dwarf system of regular shape and low surface brightness. It has been resolved into stars with the Hubble Space Telescope (HST). Judging by its CM-diagram, DDO 113 contains an old stellar population and can be classified as dSph. We have not found in it either  $HII$  regions or diffuse  $H\alpha$  emission. The measurement of its  $HI$ -flux is hampered by close neighborhood ( $\sim 10'$ ) with the bright Im-galaxy NGC 4214, a companion of which DDO 113 evidently is.

*MGC 9-20-131=CGCG 269-049.* In the central part of this dIrr galaxy a bright  $HII$  region is seen. Together with UGC 7298 it is likely to constitute a physical pair of dwarf galaxies investigated in the  $HI$  line with the Giant Metrewave Radio Telescope (GMRT) (Begum et al. 2006).

*UGC 7298 and UGC 7356.* These are irregular galaxies with a low content of  $HI$ . Their distances, 4.21 Mpc (UGC 7298) and 7.19 Mpc (UGC 7356), have recently been measured by Karachentsev et al. (2003) and Tully et al. (2007). Some faint emission regions are seen in both galaxies. Possibly, the high  $HI$ -flux from UGC 7356 is due to contamination from the bright neighboring spiral NGC 4258 since the anomalously high ratio ( $M_{HI}/L_B = 13.5M_\odot/L_\odot$ ) looks inconsistent with the morphology of this galaxy.

*IC 3308=UGC 7505.* From the Tully-Fisher relation with the  $HI$  line width  $W_{50} = 128 \text{ km s}^{-1}$  we derived the galaxy distance to be 12.8 Mpc.

*KK 144.* The measurement of  $H\alpha$ -flux is impeded because of a bright star projected near the galaxy center.

*NGC 4395.* This is a Seyfert 1 type galaxy having a star-like nucleus, which is lost among bright emission regions scattered over the disk. The integrated  $H\alpha$ -flux

in NGC 4395 as well as in the galaxies NGC 4449 and NGC 4631 was corrected for the incomplete field of view under the assumption that the  $H\alpha$ -emission in these galaxies is distributed in such a way as the blue luminosity.

*UGCA 281=Mkn 209.* On the western side of this blue compact dwarf galaxy (BCD), there is a very bright emission knot with a short arc. Judging by the distance, 5.43 Mpc, measured by Tully et al. (2007) with HST, this compact starburst galaxy has no close neighbors and is quite appropriate to be called “intergalactic *HII* region” given by Sargent & Searle (1970). We note some inconsistency in the integrated blue magnitudes for this galaxy. So, Papaderos et al. (1996) obtained  $B_T = 14.84$ , while Makarova et al. (1997) and Gil de Paz et al. (2003) give for it 15.14 and 14.15 mag, respectively. We observed UGCA 281 with the 6-m telescope in the B,V,R bands and obtained  $B_T = 14^m87 \pm 0^m05$ . This magnitude measured by M.E.Sharina is finally presented in Table 2.

*DDO 125=UGC 7577.* The diffuse emission regions in this dIrr galaxy form a knotty filament extending as far as the northern side of the galaxy.

*UGC 7584.* Together with diffuse emission regions, zones of noticeable internal absorption are seen in the galaxy, which is not typical of dwarf galaxies.

*KKH 80.* This is a galaxy of low surface brightness and of quit regular shape. In Table 2 only the upper limit of its  $H\alpha$ -flux is presented. Most likely, KKH 80 belongs to the transition dIrr/dSph type.

*NGC 4449.* The bright galaxy of Magellanic type reveals numerous powerful starburst sites scattered over the whole disk. Its emission filament structure has been described in more detail by Hunter & Gallagher (1992).

*NGC 4460.* This is a lenticular galaxy without signs of spiral structure. Surprisingly, we find a compact emission disk in its core, from which diffuse emission protuberances originated along the minor axis. Using the surface brightness fluctuations, Tonry et al. (2001) derived its distance to be 9.59 Mpc.

*NGC 4627 and NGC 4631.* This is a close in projection pair of dE and Sd galaxies with distances 9.38 Mpc and 7.66 Mpc, respectively. The elliptical component shows weak peripheral distortion, which is likely to give grounds to include this pair into the catalog of peculiar systems (Arp 1966). However, with errors in the estimation of the distances to the galaxies of  $\sim 15\%$  they may constitute a physical pair of the M32+M31 type, in which the dE component underwent “de-gasation” because of the influence of a close massive neighbor.

*KK 160.* This is a galaxy of the transition dIrr/dSph type with weak emission in *HI*, but without visible emission in the  $H\alpha$  line.

*DDO 147=UGC 7946.* This dIrr galaxy has several emission regions of different degree of compactness. Its distance, 9.9 Mpc, is estimated from the brightest stars and needs refinement.

*KK 166.* This is a dSph galaxy of very low surface brightness, for which only upper limits of the fluxes in *HI* and  $H\alpha$  are available. This is one of the faintest ( $M_B = -10.82$ ) known members of the CVnI cloud.

*UGC 7990.* The distance to this galaxy (20.9 Mpc) derived from the Tully-Fisher relation is largely different from the estimate made from its radial velocity (6.9 Mpc). The galaxy has not been resolved into stars yet.

*UGC 8215.* To the east of this dIrr galaxy there is a nearly star-like emission knot.

*NGC 5023.* This isolated late-type spiral galaxy seen almost edge-on was observed with ACS at HST by Seth et al. (2005), who estimated its distance from the TRGB luminosity to be 6.61 Mpc. All visible  $H\alpha$  emission from NGC 5023 is concentrated in its disk without signs of extraplanar gas motions.

*NGC 5195.* This is an elliptical component of the famous interacting pair M51. Its diffuse  $H\alpha$  emission is distributed over the galaxy body non-uniformly. A considerable part of the  $H\alpha$ -flux is concentrated in the circumnuclear region. Some uncertainty in the evaluation of the integrated flux from NGC 5195 is introduced by the *HII* regions of the spiral arm of NGC 5194 crossing the elliptical component of the pair.

*NGC 5229.* This is a late-type spiral galaxy seen almost edge-on. The edges of its disk are slightly curved to the opposite sides rendering the galaxy an “integral-like” shape.

*UGC 8638.* This is a compact galaxy whose main  $H\alpha$ -emission comes from several compact *HII* regions near its center.

*DDO 181=UGC 8651.* The galaxy has a curved bow-like shape similar to DDO 165. The basic  $H\alpha$ -flux in it is emitted from a very bright *HII* region at the eastern edge.

*Holmberg IV=UGC 8837.* This is an irregular galaxy whose  $H\alpha$ -emission is concentrated in compact *HII* regions without signs of a diffuse component. Judging by the distance of 6.83 Mpc measured by Tully et al. (2007), it is a satellite of the bright spiral galaxy M101.

*UGC 8882.* According to Rekola et al. (2005), this is a dE galaxy at a distance of 8.3 Mpc with a compact nucleus and without visible emission in the lines *HI* and  $H\alpha$ .

*KK 230.* This is an isolated dIrr galaxy of low surface brightness situated between the CVnI cloud and the Local Group at a distance of 1.92 Mpc. No signs of  $H\alpha$ -emission are seen. The distribution of neutral hydrogen in it with high angular resolution has been investigated by Begum et al. (2006).

*KKH 87.* This dIrr galaxy is a likely companion to M101. Almost all  $H\alpha$ -flux of it comes from compact *HII* regions without signs of a diffuse component.

*DDO 190=UGC 9240.* The periphery of the galaxy has quite a regular shape. Compact and diffuse emission knots occupy the central and southern areas of the galaxy. Being an isolated dwarf system, DDO 190 is an expressive example of a star formation burst not triggered by external tides.

*KKR 25.* This is an isolated dSph galaxy of very low surface brightness, near which a bright star is projected. KKR 25 is located between the CVnI cloud and the Local Group at a distance of 1.86 Mpc. Its radial velocity of  $+68 \text{ km c}^{-1}$  measured by Huchtmeier et al. (2003), has not been corroborated by deeper observations with GMRT (Begum & Chengalur, 2005) who estimated only the upper limit of the *HI* flux. On the northern side of KKR 25 one can see in  $H\alpha$  a faint knot, the nature of which can be established by spectral observations.

#### 4. External *SFR* comparison

In order to test our photometry, we compared the data on *SFR* from Table 2 against previous flux measurements. We have found in the literature eleven cases where  $H\alpha$ -fluxes

in the galaxies of the CVnI cloud were measured by other authors. The summary of these data is presented in Table 3 where the index “6m” at  $\log[SFR]$  corresponds to our measurements, while the index “oth” corresponds to other sources indicated in the last column. The literature  $H\alpha$ -fluxes were corrected for the external (Galactic) and internal absorption in the manner described above and reduced to the galaxy distances given in Table 2. The mean offset is  $\Delta\log[SFR] = -0.03 \pm 0.01$  in the sense that our study finds about 7% lower fluxes than literature studies, possibly due to the lower effective apertures used. The eleven points have an RMS scatter of 0.04 dex about the regression line. Given the above mentioned uncertainties and differences in reduction procedures, the agreement found in Table 3 seems to be generally good.

## 5. Discussion

As it has been noted above, the population of the CVnI cloud is distinguished among other nearby, but virialized groups by two basic features: a) most galaxies in the cloud ( $\sim 70\%$ ) do not actually interact with their closest neighbors, having negative tidal indices; b) the majority of the cloud objects ( $\sim 70\%$ ) are galaxies of low luminosity classified as  $T = 10$  (=Irr) or 9 (=Im, BCD). Evidently, both these properties are interconnected being due to the slow rate of the dynamical evolution of the CVnI volume under its low density contrast. At the present time, we have at our disposal a complete set of data on star formation rates and gas reserves in all known members of the cloud. Their  $H\alpha$  images presented in Fig.1 exhibit that galaxies of one and the same morphological type possess an enormous variety of emission patterns, being almost all under the conditions of dynamical isolation ( $TI < 0$ ). This property can be easily understood when the star formation process in galaxies, in particular its rate, is mainly governed by the internal but not the external mechanisms (tidal triggering).

The distribution of  $SFR$  for all 78 galaxies in the CVnI cloud as a function of their blue absolute magnitude is presented in Fig.2 by filled circles. The galaxies with only the upper limit of the  $H\alpha$ -flux are given by open circles. For comparison, we draw here similar data on the complete set of 41 galaxies situated in the nearby virialized group around M81 (Karachentsev & Kaisin, 2007). They are shown in this diagram by filled and open squares. As can be seen, the bright members of the cloud and the group follow a common linear relationship  $SFR \propto L_B$  displayed by the line. The differences between the samples are not large both from the integrated  $SFR$  range and from the scatter of specific  $SFR$  per unit luminosity. Faint dwarfs in the two samples with  $M_B > -13^m$  demonstrate a systematic offset from the main sequence. However, their displacement in  $SFR$  can be essentially reduced in a new scenario of stellar evolution proposed by Weidner & Kroupa, 2005.

Another important diagram (Fig.3) illustrates a relationship between  $SFR$  and total hydrogen mass  $M_{HI}$  of galaxies. The members of the CVnI cloud and those of M81 group are shown here by the same symbols as in Fig.2. As have been already noted by many authors: Kennicutt (1989, 1998), Taylor & Webster (2005), Tutukov (2006), spiral and irregular galaxies show a steeper dependence of  $SFR$  on  $M_{HI}$  than on luminosity  $L_B$ , namely  $SFR \propto M_{HI}^{1.5}$ . This testifies that dIrr galaxies preserve a relatively larger amount of gas than spirals to maintain star formation with

the now observed rates. This diagram also shows that the members of the CVnI cloud and M81 group are mutually well mixed as in the previous plot.

To estimate the evolutionary status of normal and dwarf galaxies in the CVnI cloud, we used the data on dimensionless parameters in the last two columns of Table 2:  $p_* = \log[(SFR)T_0/L_B]$  and  $f_* = \log[M_{HI}/(SFR)T_0]$ , which characterize the past and future of the star formation process in a galaxy on the assumption of permanent star formation rate. The evolutionary “past-future” diagram for the observed galaxies is presented in Fig.4. The members of the CVnI cloud are shown by circles, and the members of the group M81 are marked by squares. The open symbols correspond to the cases where observations give only the upper limit of the flux in  $H\alpha$  or  $HI$ .

The distribution of galaxies in the diagnostic  $\{p_*, f_*\}$  diagram shows some interesting properties. The members of the CVnI cloud, on the whole, are located symmetrically enough with respect to the origin of coordinates, having median values  $p_* = +0.02$  and  $f_* = -0.03$ . This means that the observed star formation rates in the CVnI galaxies proved to be quite sufficient to reproduce their observed luminosity (baryon mass). Moreover, the cloud galaxies possess gas reserves sufficient to maintain the observed star formation rates during one more Hubble time  $T_0$ , being just in the middle of their evolutionary path. For comparison, the median values  $p_*$  and  $f_*$  for the M81 group members are  $-0.30$  and  $+0.12$ , respectively, i.e. their typical value of  $SFR$  per unit luminosity is twice as low as in the galaxies of CVnI. But this difference is easily explicable by the presence around M81 of a lot of dSphs in which the current star formation can be suppressed by tidal stripping. The CVnI cloud contains only 3 or 4 such “extinct” dwarfs: KK109, DDO113, KK166 and, probably, UGC8882.

In contrast to spiral galaxies, dIrr galaxies of low luminosity exhibit multiple episodes of global star formation (Dohm-Palmer et al. 2002, Dolphin et al. 2003, Skillman 2005, McConnachie et al. 2005, Young et al. 2007). Stinson et al. 2007 simulated the collapse of isolated dwarf galaxies with the effects of supernova feedback and showed that star formation in them occurs in the form of bursts rather than in the mode of a sluggish process. The observed  $H\alpha$  flux in galaxies represents its current  $SFR$  only over the past  $\sim 10$  Myr (Bell & Kennicutt, 2001, Annibali et al. 2007). The difference between the observed “momentary” and the secular value of  $SFR$  averaged over  $T_0$  will lead to scatter of flashing and dimming dIrr galaxies in the diagram  $\{p_*, f_*\}$  along the diagonal line  $p_* = -f_*$ . This tendency is actually seen in Fig.4 both for the CVnI cloud and for the M81 group members. These data permit us to estimate that the global star formation rate in the dIrrs can be varied with time by about an order of magnitude. The most expressive representatives of a dwarf galaxy at a burst stage are UGCA 281=Mkn209 and UGC 6541=Mkn178, in which the specific  $SFR$  per unit luminosity is 16 times and 7 times higher than the average value. The known “exploding” galaxy M82 in the M81 group has a bit lower specific  $SFR$ .

Among 500 galaxies of the Local volume there are only 6 galaxies with the hydrogen mass-to-luminosity ratio greater  $5 M_\odot/L_\odot$ . Surprisingly, half of these semi-gaseous galaxies: DDO 154, NGC 3741 and UGCA 292 reside in the CVnI cloud. All three of them are located in the upper right quadrant of Fig.4. Considering the M81 group, Karachentsev &

Kaisin (2007) have found in this quadrant only one peculiar object, the dark  $HI$  cloud HIJASS with a rather uncertain estimate of  $SFR$ . Probably, galaxies start their evolution just from this quadrant, [ $p_* > 0, f_* > 0$ ], converting their initial gaseous mass into stars.

There is a widespread point of view that close galaxy encounters trigger enhanced star formation in them. However, Hunter & Elmegreen, 2004 and Noeske et al. 2001 find no correlation between star formation activity in galaxy and its proximity to other neighboring galaxies. Telles & Maddox, 2000 and James et al. 2004 found that bursting dwarf galaxies inhabit slightly lower density environments than those of denser field. Our data are in agreement with such a conclusion. The left-hand diagram of Fig.5 presents the distribution of members of the CVnI cloud (circles) and of the M81 group (squares) versus their specific  $SFR$  and tidal index. Here the solid regression line has a slope of  $(-0.01 \pm 0.03)$  corresponding to the galaxies detected in the  $H\alpha$  line, while the dashed regression line with a slope of  $(-0.07 \pm 0.05)$  corresponds to the whole sample of 78+41 galaxies including those with upper limits of their  $H\alpha$  flux. This diagram does not show significant difference in  $SFR$  for galaxies in groups ( $TI > 0$ ) as compared to isolated ones. In particular, the strongly disturbed system Garland near NGC 3077 and the isolated blue galaxy UGCA 281 have almost the same extremely high values of  $p_*$ .

The right diagram of Fig.5 presents the time of exhaustion of the available reserves of  $HI$  gas,  $f_*$ , for the CVnI cloud and the M81 group galaxies versus their tidal index. The solid and dashed regression lines with slopes  $(-0.10 \pm 0.04)$  and  $(-0.01 \pm 0.05)$  correspond to the galaxies detected in the  $H\alpha$  and  $HI$  lines, and to the whole sample of galaxies, respectively. Despite the considerable dispersion, a trend of diminishing of the value of  $f_*$  from isolated galaxies towards interacting ones is seen, which reflects the known tendency of rising  $HI$ -deficiency with increasing density of its environment (Giovanelli & Haynes, 1991).

We regard the isolated ( $TI = -0.7$ ) lenticular galaxy NGC 4460 to be the most intriguing object in the considered sample. A powerful star formation burst in its center exhasts all available reserve of gas just for 170 Myr. Possibly, we observe here a rare event of interaction of the S0 galaxy with an intergalactic  $HI$  cloud. Such dark completely starless clouds have already been detected in the nearby groups M81 (Boyce et al. 2001), Leo-I (Schneider 1985) and the nearby Virgo cluster (Minchin et al. 2005).

## 6. Conclusions

A systematic survey of  $H\alpha$ -emission in the nearest scattered cloud CVnI shows that in most of its galaxies the process of active star formation is on despite the low density contrast of this cloud and rather rare interaction between its members. By making full use of our  $H\alpha$ -survey, we can estimate the mean density of  $SFR$  in the cloud. A conical volume in the distance range from 2 to 10 Mpc, resting in a sky region of  $\sim 1500$  square degrees, makes 153  $Mpc^3$ . In this volume we have a summary value  $\Sigma(SFR) = 18.6 M_\odot yr^{-1}$ , which yields an average density of star formation rate  $\dot{\rho}_{SFR} = 0.12 M_\odot yr^{-1} Mpc^{-3}$ . The obtained value turns out to be a little less than  $\dot{\rho}_{SFR} = 0.165 M_\odot yr^{-1} Mpc^{-3}$  for a “sell of homogeneity” embracing the group M81 (Karachentsev & Kaisin, 2007). According

to Nakamura et al. (2004), Martin et al. (2005) and Hanish et al. (2006), the average star formation rate per 1  $Mpc^3$  at the present epoch ( $z=0$ ) is  $(0.02-0.03) M_\odot yr^{-1} Mpc^{-3}$ . Consequently, the CVnI cloud has excess of  $SFR$  density 4–6 times higher in comparison with the mean global quantity, which roughly corresponds to the cloud density contrast on the sky,  $\Delta N/N \sim 4$ . Herefrom we conclude that the CVnI cloud is characterised by a usual norm of star formation in its galaxies.

*Acknowledgements.* We would like to thank Margarita Sharina for her help with the photometry of UGCA 281. We are also grateful to B. Tully for useful discussions. Support associated with HST program 10905 was provided by NASA through a grant from the Space Telescope Science Institute, which is operated by the Association of Universities for Research in Astronomy, Inc., under NASA contract NAS5-26555. This work was also supported by RFFI grant 07-02-00005 and grant DFG-RFBR 06-02-04017.

## References

- Afanasiev V.L., Gazhur E.B., Zhelenkov S.R. & Moiseev A.V. 2005, Bull.SAO, 58, 90  
 Annibali F., Aloisi A., Mack J. et al. 2007, astro-ph/0708.0852  
 Arp H. 1966, Atlas of Peculiar Galaxies, ApJS, 14, 1  
 Begum A. & Chengalur J.N. 2005, MNRAS, 362, 609  
 Begum A., Chengalur J.N., Karachentsev I.D., Kaisin S.S. & Sharina M.E. 2006, MNRAS, 365, 1220  
 Bell E.F. & Kennicutt R.C. 2001, ApJ, 548, 681  
 Boyce P.J., Minchin R.F., Kilborn V.A. et al. 2001, ApJ, 560, L127  
 de Vaucouleurs, G., de Vaucouleurs, A., Corwin, A., Buta, R.J., Paturel, G., Fouqué, P. 1991, Third Reference Catalogue of Bright Galaxies, New-York - Springer-Verlag  
 de Vaucouleurs, G. 1975, in “Galaxies and the Universe,” Sandage A., Sandage M., Kristian J. (eds.) Chicago, Univ. of Chicago Press, p. 557  
 Dohm-Palmer R.C. et al. 2002, AJ, 123, 813  
 Dolphin A.E. et al. 2003, AJ, 126, 187  
 Gallagher J.S., Hunter D.A. & Tutukov A.V. 1984, ApJ, 284, 544  
 Gil de Paz, Madore B.F. & Pevunova O. 2003, ApJS, 147, 29  
 Giovanelli R. & Haynes M.P. 1991, ARA&A, 29, 499  
 Hanish D.J., Meurer G.R., Ferguson H.C. et al. 2006, ApJ, 649, 150  
 Hodge P.W. & Kennicutt R.C. 1983, AJ, 88, 296  
 Hoopes C.G., Walterbos R.A.M. & Rand R.J. 1999, ApJ, 522, 669  
 Huchtmeier W.K., Karachentsev I.D. & Karachentseva V.E. 2003, A&A, 401, 483  
 Huchtmeier W.K., Karachentsev I.D., Karachentseva V.E. & Ehle M. 2000, A&AS, 141, 469  
 Hunter D.A. & Elmegreen B.G. 2004, AJ, 128, 2170  
 Hunter D.A. & Gallagher J.S. 1992, ApJ, 391, L9  
 James P.A., Shane N.S., Beckman J.E., et al. 2004, A&A, 414, 23  
 Karachentsev I.D. & Kaisin S.S. 2007, AJ, 133, April  
 Karachentsev I.D., Dolphin A.E., Tully R.B. 2006, AJ, 131, 1361  
 Karachentsev I.D., Karachentseva V.E., Huchtmeier W.K., Makarova D.I. 2004, AJ, 127, 2031  
 Karachentsev I.D., Sharina M.E., Dolphin A.E. 2003, A&A, 398, 467  
 Karachentsev I.D. 1966, Astrofizika, 2, 81  
 Kennicutt R.C. 1998, ApJ, 498, 541  
 Kennicutt R.C. 1989, ApJ, 344, 685  
 Kennicutt R.C., Edgar B.K., Hodge P.W. 1989, ApJ, 337, 761  
 Makarova L.N., Karachentsev I.D. & Georgiev T.B. 1997, Astron. Lett., 23, 435  
 Martin D.C., Seibert M., Buat V. et al. 2005, ApJ, 619, 59  
 McConnachie A.W., Arimoto N., Irwin M., Tolstoy E. 2006, MNRAS, 373, 715  
 Miller B.W. & Hodge P. 1994, ApJ, 427, 656  
 Minchin R.F., Davies J., Disney M. et al. 2005, ApJ, 622, L21  
 Nakamura O., Fukugita M. et al. 2004, AJ, 127, 2511  
 Oke J.B. 1990, AJ, 99, 1621  
 Papaderos P. et al. 1996, A&AS, 120, 207  
 Rekola R., Jerjen H. & Flynn C. 2005, A&A, 437, 823  
 Sargent W.L.W. & Searle L. 1970, ApJ, 162, L155  
 Seth A.C., Dalcanton J.J. & de Jong R.S. 2005, AJ, 129, 1331  
 Schlegel D.J., Finkbeiner D.P. & Davis M. 1998, ApJ, 500, 525  
 Schneider S.E. 1985, ApJ, 288, L33

- Skillman E.D. 2005, *New Astronomy Review*, 49, 453  
Spergel D.N. et al. 2003, *ApJS*, 148, 175  
Stinson G.S., Dalcanton J.,J., Quinn T. et al. 2007, *astro-ph/0705.4494*  
Strickland D.K., Heckman T.M., Colbert E.J.M. et al. 2004, *ApJ*, 606, 829  
Taylor E.N. & Webster R.L. 2005, *ApJ*, 634, 1067  
Telles E. & Maddox S. 2000, *MNRAS*, 311, 307  
Tonry J.L. et al. 2001, *ApJ*, 546, 681  
Tully R.B., Shaya E.J. & Pierce M.J. 1992, *ApJS*, 80, 479  
Tully R.B. et al. 2007, in preparation  
Tully R.B. 1988, *Nearby Galaxy Catalog*, Cambridge Univ. Press  
Tutukov A.V. 2006, *Astronomy Reports*, 50, 526  
van Zee L. 2000, *AJ*, 119, 2757  
Vennik J. 1984, *Tartu Astron. Obs. Publ.* 73, 1  
Verheijen M.A.W. 2001, *ApJ*, 563, 694  
Weidner C. & Kroupa P. 2005, *ApJ*, 625, 754  
Young J.S., Allen L., Kenney J.D. & Rownd B. 1996, *AJ*, 112, 1903  
Young L.M., Skillman E.D., Weisz D.R. & Dolphin A.E. 2007, *ApJ*, 659, 331

**Table 1.** The observational Log

Galaxy	Date	$T_{exp}$
U5427	03/02/2005	1200
N3344	04/02/2005	300
KK109	05/02/2005	1200
BTS76	04/02/2005	1200
MCG6-27-17	05/02/2005	1200
DDO113	27/01/2004	1200
MCG9-20-131	06/02/2005	1200
U7298	06/02/2005	900
U7356	05/02/2005	1200
I3308	04/02/2005	600
KK144	04/02/2005	1200
N4395	06/02/2005	300
UA281	24/05/2006	300:
DDO125	18/05/2005	1200
U7584	04/02/2005	1200
KKH80	04/02/2005	1200
N4449	24/05/2006	500
DDO127	05/02/2005	1200
U7605	05/02/2005	1200
N4460	06/02/2005	600
KK149	06/02/2005	1200
U7639	06/02/2005	1200
KK151	06/02/2005	1200
N4627	06/02/2005	600
N4631	22/05/2006	900:
KK160	22/03/2006	1200:
DDO147	05/02/2005	1200
KK166	22/03/2006	1200:
U7990	05/02/2005	1200
U8215	16/05/2005	1200
N5023	04/02/2005	600
N5195	05/05/2005	500
U8508	17/03/2001	1200
N5229	06/02/2005	1200
U8638	06/02/2005	1200
DDO181	24/05/2006	500
Holmberg IV	29/01/2004	600
U8882	21/03/2006	1200:
KK230	03/02/2005	1200
KKH87	29/01/2004	1200
DDO190	24/05/2006	400
KKR25	25/03/2001	600:

**Table 2.** Basic parameters of galaxies in the Canes Venatici I cloud.

Name	RA (J2000) Dec	T	$TI$	$V_{LG}$	$D$ Mpc	$M_B$ mag	$\log M_{HI}$ $M_{\odot}$	$\log F$	$\log SFR$ $M_{\odot} \text{ yr}^{-1}$	$p_*$	$f_*$
(1)	(2,3)	(4)	(5)	(6)	(7)	(8)	(9)	(10)	(11)	(12)	(13)
U5427	100441.0+292159	8	-1.2	424	7.1	-14.48	7.49	-13.03	-2.19	0.00	-0.46
U5672	102820.9+223417	10	-0.7	428	6.3	-14.65	7.40	a	-2.10	0.02	-0.64
N3274	103217.1+274007	6	-0.3	461	6.5	-16.16	8.74	a	-1.11	0.41	-0.29
N3344	104330.2+245525	4	-1.5	498	6.9	-19.03	9.67	-11.09	-0.26	0.11	-0.21
U6541	113329.1+491417	10	-0.7	304	3.89	-13.71	7.03	b	-1.68	0.82	-1.43
N3738	113548.6+543122	10	-1.0	305	4.90	-16.61	8.09	a	-1.30	0.04	-0.75
N3741	113606.4+451707	10	-0.8	264	3.03	-13.13	8.05	a	-2.28	0.45	0.19
KK109	114711.2+434019	-1	-0.6	241	4.51	-9.73	6.52	-15.7:	-5.3:	-1.2:	1.6:
DDO99	115053.0+385250	10	-0.5	248	2.64	-13.52	7.71	a	-2.48	0.09	0.05
BTS76	115844.1+273506	10	-1.2	451	6.3	-12.60	7.0:	-14.17	-3.45	-0.51	0.3:
N4068	120402.4+523519	10	-1.0	290	4.31	-15.07	8.13	a	-1.65	0.30	-0.36
MCG627	120956.4+362607	10	0.6	341	4.7	-12.97	6.7:	-14.09	-3.62	-0.83	0.2:
N4144	120959.3+462726	6	0.9	319	7.41	-17.64	8.79	a	-0.71	0.21	-0.64
N4163	121208.9+361010	9	1.4	164	2.96	-13.81	7.29	a	-2.83	-0.37	-0.02
N4190	121344.6+363760	10	0.0	234	3.5	-14.33	7.83	a	-2.10	0.15	-0.21
DDO113	121457.9+361308	-1	1.6	283	2.86	-11.67	6.3:	-15.0:	-5.0:	-1.6:	1.1:
N4214	121538.9+361939	9	-0.7	295	2.94	-17.19	8.79	c	-0.64	0.46	-0.71
MCG920	121546.7+522315	10	-0.7	245	3.4	-12.46	7.10	-13.17	-2.98	0.02	-0.07
U7298	121628.6+521338	10	-0.7	255	4.21	-12.27	7.31	-14.49	-4.12	-1.05	1.29
N4244	121729.9+374827	6	-0.0	255	4.49	-18.60	9.30	d	-0.90	-0.36	0.06
N4258	121857.5+471814	4	-0.7	507	7.83	-21.25	9.81	e	0.35	-0.17	-0.68
U7356	121909.1+470523	10	0.4	330	7.19	-13.61	8.7:	-14.64	-3.81	-1.27	2.4:
I3308	122517.9+264253	7	-2.:	277	12.8	-15.55	8.68	-13.10	-1.68	0.08	0.17
KK144	122527.9+282857	10	-0.9	453	6.3	-12.59	7.90	-13.83	-3.11	-0.17	0.87
N4395	122549.8+333246	8	0.1	315	4.67	-17.88	9.22	-11.04	-0.56	0.27	-0.36
UA281	122616.0+482931	9	-0.8	349	5.43	-13.86	7.84	-11.80	-1.21	1.22	-1.09
DDO126	122705.1+370833	10	0.1	231	4.87	-14.38	8.20	a	-1.91	0.32	-0.03
DDO125	122741.8+432938	10	-0.9	240	2.54	-14.16	7.52	-12.67	-2.74	-0.42	0.12
U7584	122802.9+223522	9	-0.1	545	7.6	-13.30	7.59	-13.39	-2.50	0.16	-0.05
KKH80	122805.4+221727	10	-0.1	542	7.5	-12.47	7.02	-15.4:	-4.5:	-1.5:	1.4:
N4449	122811.2+440540	9	-0.0	249	4.21	-18.27	9.52	-10.43	-0.03	0.64	-0.59
DDO127	122828.5+371400	9	-0.7	291	6.9	-14.28	8.15	-13.64	-2.84	-0.57	0.85
U7605	122839.0+354305	10	0.7	317	4.43	-13.53	7.42	-12.90	-2.49	0.08	-0.23
N4460	122845.8+445152	1	-0.7	542	9.59	-17.89	7.65	-11.72	-0.59	0.23	-1.90
KK149	122852.3+421040	10	-0.8	446	6.2	-14.06	7.43	-13.39	-2.68	-0.32	-0.03
U7639	122953.0+473148	10	0.4	446	7.1	-15.18	7.79	-13.64	-2.82	-0.91	0.47
KK151	123023.8+425405	9	-0.4	479	6.7	-13.41	7.32	-13.60	-2.83	-0.21	0.01
DDO133	123253.0+313221	10	-1.1	321	6.1	-15.47	8.58	c	-1.53	0.26	-0.03
Arp211	123721.3+384443	10	-0.7	484	6.70	-13.47	7.13	b	-2.46	0.13	-0.55
UA292	123840.0+324600	10	-0.3	306	5.0	-12.47	7.93	f	-2.19	0.80	-0.02
N4627	124159.7+323425	-3	-1.4:	541	9.38	-16.87	7.6:	-15.0:	-3.9:	-2.7:	1.4:
N4631	124208.0+323229	7	-1.1:	605	7.66	-19.74	10.11	-11.04	0.37	0.45	-0.40
I3687	124215.1+383007	10	1.1	385	4.57	-14.64	8.03	a	-2.05	0.07	-0.06
KK160	124357.4+433941	10	1.0	346	4.8	-11.52	6.58	-15.1:	-4.6:	-1.3:	1.1:
DDO147	124659.8+362835	10	-1.4	351	9.9	-14.94	8.62	-13.26	-2.15	-0.15	0.63
KK166	124913.3+353645	-3	0.3		4.74	-10.82	6.4:	-15.15:	-4.7:	-1.0:	0.9:
U7990	125027.0+282107	10	-2.:	495	20.9	-15.46	8.38	-14.01	-2.25	-0.45	0.49
N4736	125053.5+410710	2	-0.5	353	4.66	-19.83	8.68	e	-0.19	-0.14	-1.27
DDO154	125405.2+270855	10	-1.1	355	3.91	-13.87	8.72	a	-2.08	0.35	0.66
N4826	125644.2+214105	2	-0.6	364	4.44	-19.77	8.42	g	-0.54	-0.47	-1.18
I4182	130549.3+373621	9	0.6	356	4.70	-16.40	8.53	a	-1.61	-0.19	0.00
U8215	130803.6+464941	10	-0.3	297	4.55	-12.30	7.32	-13.77	-3.34	-0.28	0.52
N5023	131211.9+440219	6	-1.6	476	6.61	-17.12	8.70	-12.03	-1.11	0.02	-0.33
DDO167	131322.8+461911	10	0.0	243	4.19	-12.70	7.27	c	-2.64	0.26	-0.23
DDO168	131428.6+455510	10	-0.0	273	4.33	-15.28	8.42	a	-1.83	0.04	0.11
DDO169	131530.7+472947	10	-0.2	345	4.23	-13.71	7.81	a	-2.40	0.10	0.07
N5204	132936.4+582504	9	-1.1	341	4.65	-16.75	8.76	a	-1.04	0.24	-0.34
N5194	132956.0+471404	5	4.1	555	8.0	-21.34	9.52	g	0.56	0.00	-1.18
N5195	132958.7+471605	-1	5.0	558	8.02	-19.22	8.18	-11.33	-0.38	-0.09	-1.58
U8508	133044.4+545436	10	-1.0	186	2.56	-12.98	7.34	-12.51	-2.57	0.22	-0.23



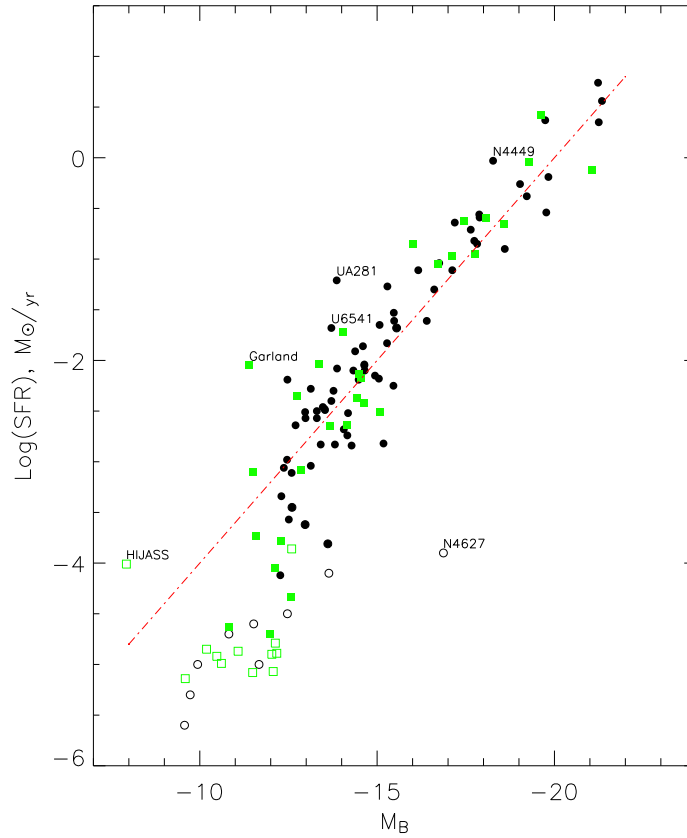
Name	RA (J2000) Dec	T	$TI$	$V_{LG}$	$D$ Mpc	$M_B$ mag	$\log M_{HI}$ $M_{\odot}$	$\log F$	$\log SFR$ $M_{\odot} \text{ yr}^{-1}$	$p_*$	$f_*$
(1)	(2,3)	(4)	(5)	(6)	(7)	(8)	(9)	(10)	(11)	(12)	(13)
N5229	133402.9+475455	7	-0.6	460	5.1	-14.60	8.18	-12.46	-1.86	0.28	-0.10
N5238	133442.7+513650	9	-0.9	345	4.24	-14.64	7.27	a	-2.04	0.08	-0.83
U8638	133919.4+244633	9	-1.3	273	4.27	-13.77	7.22	-12.68	-2.30	0.17	-0.62
DDO181	133953.8+404421	10	-1.3	272	3.02	-12.97	7.39	-12.58	-2.51	0.28	-0.24
DDO183	135051.1+380116	10	-1.2	257	3.18	-13.13	7.36	a	-3.04	-0.31	0.26
HolmIV	135445.1+535417	10	0.6	276	6.83	-15.48	8.34	-12.40	-1.61	0.18	-0.19
U8833	135448.7+355015	10	-1.4	285	3.12	-12.37	7.14	e	-3.06	-0.03	0.06
U8882	135714.6+540603	-1	0.0		8.3	-13.64	7.2:	-15.04:	-4.1:	-1.6:	1.2:
M101	140312.8+542102	6	0.6	379	7.38	-21.23	10.36	e	0.74	0.23	-0.52
N5474	140502.1+533947	8	2.0	413	7.2	-17.74	9.12	a	-0.82	0.06	-0.20
N5477	140533.1+542739	9	1.4	443	7.7	-15.29	8.26	a	-1.27	0.59	-0.61
KK230	140710.7+350337	10	-1.0	126	1.92	-9.57	6.35	-15.32:	-5.6:	-1.5:	1.85:
KKH87	141509.4+570515	10	1.0	473	7.4	-13.30	7.64	-13.42	-2.57	0.09	0.07
DDO187	141556.5+230319	10	-1.2	172	2.28	-12.51	7.16	a	-3.57	-0.59	0.59
N5585	141948.3+564349	4	-0.8	459	5.7	-17.82	8.98	a	-0.85	0.00	-0.31
DDO190	142443.5+443133	10	-1.3	263	2.79	-14.18	7.63	-12.53	-2.52	-0.21	0.01
DDO194	143524.6+571524	10	-0.0	385	8.0	-15.05	8.00	a	-2.18	-0.22	0.04
KKR25	161347.6+542216	-1	-0.7	68:	1.86	-9.94	4.9:	-14.64:	-5.0:	-1.0:	-0.2:

**NOTES**

- a – James et al., 2004,  
b – Gil de Paz et al., 2003,  
c – Hunter & Elmegreen, 2004,  
d – Strickland et al., 2004,  
e – Kennicutt et al., 1989  
f – van Zee, 2000  
g – Young et al., 1996.

**Table 3.** Comparison of SFR estimates for the CVnI galaxies

Galaxy	$\log(\text{SFR})_{6m}$	$\log(\text{SFR})_{oth}$	$\Delta$	Source
NGC4395	-0.56	-0.59	0.03	Kennicutt et al. 1989
UGCA281	-1.21	-1.19	-0.02	Gil de Paz et al. 2003
DDO125	-2.74	-2.72	-0.02	Hunter & Elmegreen 2004
NGC4449	-0.03	0.01	-0.04	Kennicutt et al. 1989
NGC4631	0.37:	0.42	-0.05	Hoopes et. 1999
NGC4631	0.37:	0.41	-0.04	Kennicutt et al. 1989
UGC8508	-2.57	-2.51	-0.06	James et al. 2004
DDO181	-2.51	-2.47	-0.04	van Zee 2000
HolmbergIV	-1.61	-1.57	-0.04	James et al. 2004
DDO190	-2.52	-2.43	-0.09	James et al. 2004
DDO190	-2.52	-2.56	0.04	van Zee 2000

**Fig. 2.** Star formation rate versus blue absolute magnitude for 78 galaxies in the Canes Venatici I cloud (circles) and 41 members of the M81 group (squares). The open symbols indicate the galaxies with only upper limit of their  $SFR$ . The line corresponds to a constant  $SFR$  per unit luminosity.

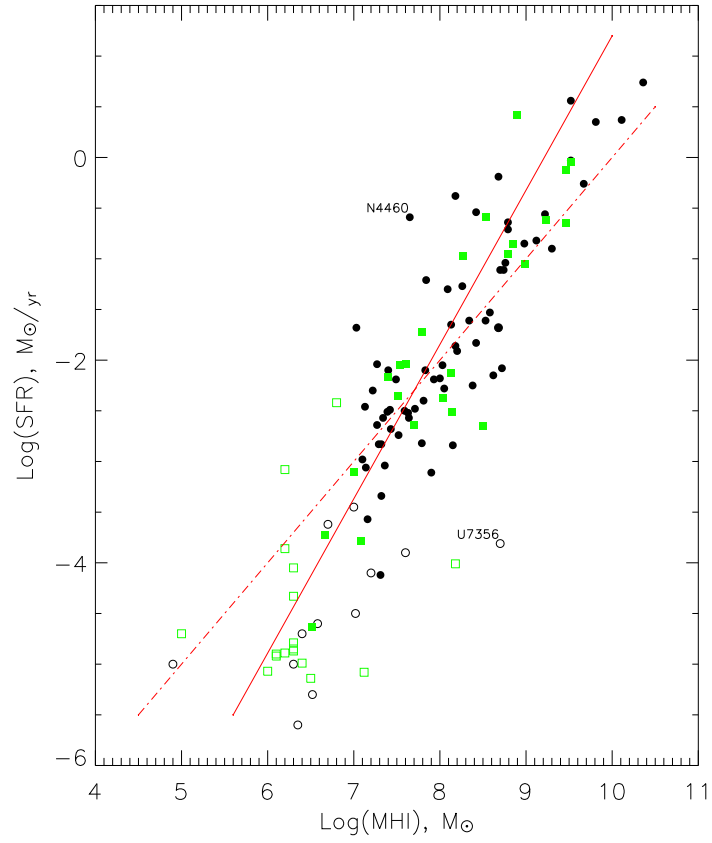


**Fig. 3.** Star formation rate versus neutral hydrogen mass for galaxies in the CVnI cloud (circles) and the M81 group (squares). The galaxies with upper limit of  $SFR$  or  $M_{HI}$  are indicated by open symbols. The dashed line corresponds to a fixed  $SFR$  per unit hydrogen mass and the solid line traces the relationship  $SFR \propto M_{HI}^{1.5}$ .

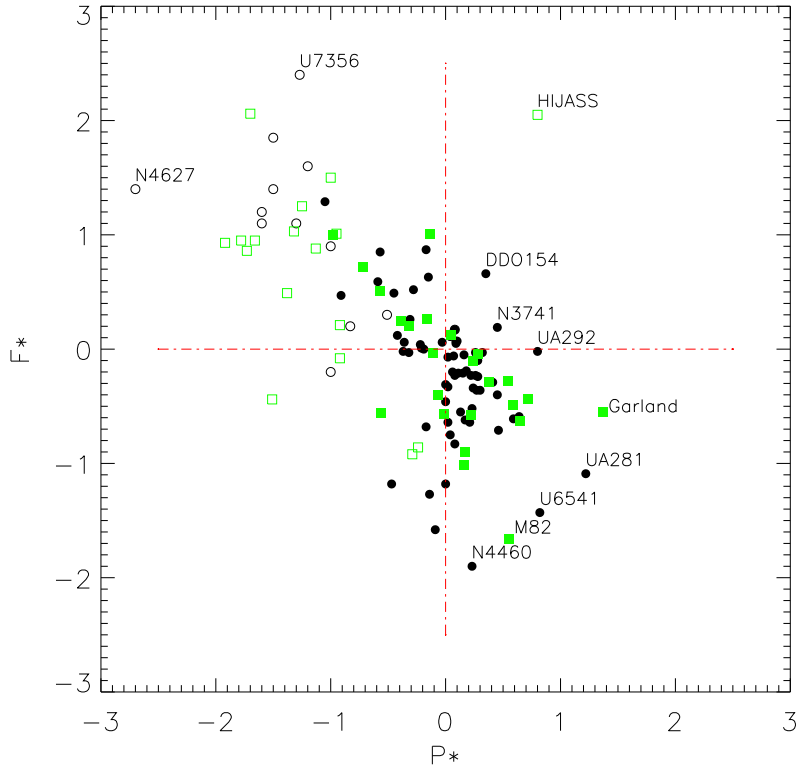


**Fig. 4.** The CVnI cloud galaxies and the M81 group members on the evolutionary plane “past-future”:  $p_* = \log([SFR] \cdot T_0 / L_B)$  and  $f_* = \log(M_{HI} / [SFR] \cdot T_0)$ . The galaxies with upper limits of  $SFR$  or  $M_{HI}$  are shown by open symbols.

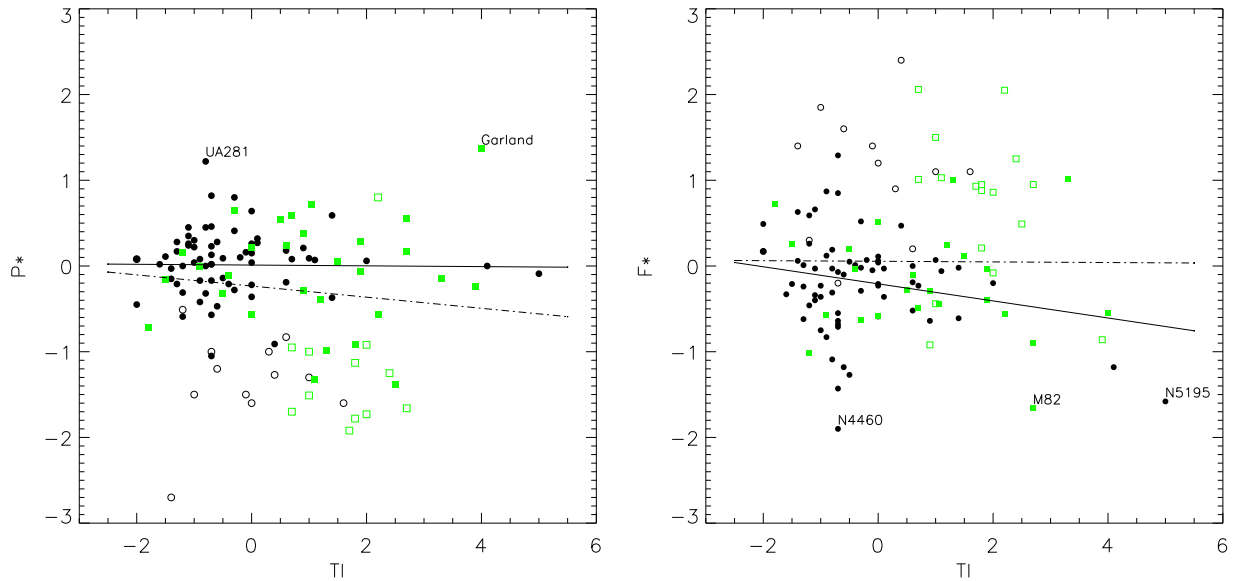


**Fig. 5.** The specific star formation rate (*left*) and the time of exhaustion of the available reserves of gas (*right*) versus the tidal index for the CVnI cloud (circles) and the M81 group galaxies (squares). The open symbols indicate the galaxies with upper limits of  $SFR$  or  $M_{HI}$ . The solid and dashed regression lines correspond to the filled only and to the filled plus open symbols, respectively.